ORIGINAL PAPER

Aeroacoustic wind tunnel design

J. Pereira Gomes[1] · A. Bergmann[1] · H. Holthusen[2]

Abstract

Further progress in airframe noise research including noise prediction and noise reduction solutions depends on the availability of aeroacoustic wind tunnel test facilities with superior aerodynamic and acoustic quality. The demand for aeroacoustic wind tunnels with extremely low background noise and pressure fluctuations, yet with a relevant test section cross-section area and flow velocity, increased significantly over the last decade. In the future, this demand will continue to grow to cope with the challenging noise reduction objectives for aviation noise defined for the years to come. The present text is focused on the state-of-the-art aeroacoustic wind tunnels available today and their design. The design guidelines discussed here assume a classic aerodynamic wind tunnel as a baseline. Therefore, the present text is addressed to both those who are interested in the design of a completely new aeroacoustic wind tunnel as well as those interested in the acoustic upgrade of an existing aerodynamic wind tunnel. As a direct consequence of the multi-disciplinary nature of this complex task, and the multitude of solutions and design tools that are required to complete it, the approach followed here subdivides the design of the aeroacoustic wind tunnel into four main sections: wind tunnel airline circuit (includes the first and second airline cross legs), drive unit and anechoic plenum. While the design approach for the airline circuit and the drive unit is strongly based on coupled numerical solutions of CFD and acoustic solvers, the design of the acoustic plenum gives more emphasis to in situ observations and to experimental results. The main sections of the aeroacoustic wind tunnel and their best design are discussed separately in this contribution.

List of symbols

A	Area, m^2
A_0	Reference area (= 1 m^2), m^2
A_p	Wall partition area, m^2
c	Speed of sound, m/s
$C_{p,\text{RMS}}$	Pulsating coefficient
d	Duct diameter, m
f	Frequency, Hz
h	Brightness per histogram level
κ	Ratio of specific heats
L	Length, m
l	Duct length, m
l_{ef}	Effective duct length, m
L_m	Overall brightness level
L_p	Sound pressure level
$L_{p,\text{OSPL}}$	Overall sound pressure level
Δf	Frequency bandwidth, Hz
ΔL_p	Acoustic damping
Δp_{loss}	Pressure loss
λ	Wavelength, m
$\dot{m}$	Mass flow rate, kg/s
Ma	Mach number
p	Pressure, N/m^2
p_0	Reference pressure (= 20 μPa), N/m^2
p_{tot}	Total pressure, N/m^2
r	Distance, m
r_0	Offset of the acoustic centre along the measurement path, m
R'_I	Apparent intensity sound reduction index

✉ J. Pereira Gomes
   jorge.gomes@dnw.aero

   A. Bergmann
   andreas.bergmann@dnw.aero

   H. Holthusen
   hermann.holthusen@dnw.aero

1   German-Dutch Wind Tunnels (DNW), Lilienthalplatz 7, 38108 Braunschweig, Germany

2   German-Dutch Wind Tunnels (DNW), Voorsterweg 31, 8316 PR Marknesse, The Netherlands

ρ	Flow density, kg/m^3
U	Flow velocity, m/s
V	Volume, m^3

Abbreviations

ARC	Active resonance control
atm	Atmospheric
BBN	Broadband noise
BPF	Blade passing frequency
CFD	Computational fluid dynamics
DLR	German Aerospace Centre
DNW	German–Dutch Wind Tunnels foundation of DLR and NLR
in	Inlet
inc	Incident
LLF	Large low-speed facility
NLR	Netherlands Aerospace Centre
NWB	Low speed wind tunnel Braunschweig
OSPL	Overall sound pressure level
out	Outlet
SPL	Sound pressure level
trs	Transmitted

1 Introduction

The design process of an aeroacoustic wind tunnel, with rare exceptions, is very complex, as are the multi-physical disciplines required to guarantee a successful design. The complexity of such design is further increased, because it is absolutely essential that a good acoustically oriented wind tunnel should provide superior aerodynamic characteristics as well. In this respect, an ideal aeroacoustic wind tunnel must offer the possibility of testing in a closed test section to guarantee the best representation of the flow field, and also in an open or partially open test section to measure the complete acoustic far field generated by the test model in free-field conditions. From the mere point of view of the acoustic design, the requirements for the background noise level in the wind tunnel test section and its spectral distribution are primarily defined by the size of the wind tunnel and by the type of acoustic tests to be performed. In large wind tunnels dedicated to full-scale model testing, the sound frequency range below 4 kHz is of special interest. For smaller models, such as 1 / 10 scaled models, the sound frequency range between 10 and 40 kHz is of more importance. Because this is a very common model scale tested in mid-sized wind tunnels, their design should be optimized to this frequency range [12]. More silent aerofoils, such as those designed for wind turbines, require extremely low background noise levels in the test section and the surrounding chamber to maximize the signal-to-noise ratio of the experimental results. In contrast, aircraft models in high-lift configuration are typically much noisier and consequently more forgiving of the background noise around them.

The current contribution approaches the aeroacoustic wind tunnel design under the assumption that the reader is familiar with the design of classic aerodynamic wind tunnels. This way, instead of covering the design of an aeroacoustic wind tunnel from scratch, the present contribution discusses the major guidelines for providing an aerodynamic wind tunnel with excellent acoustic capabilities. It discusses the upgrade of a classic design of an aerodynamic wind tunnel into an optimized aeroacoustic wind tunnel design, using the low-speed wind tunnel DNW-NWB as example.

In the approach suggested here, the wind tunnel design is subdivided into four major sections that can be designed independently (see Fig. 1). For the design of both cross legs of the airline circuit, an interactive optimization approach that combines CFD tools and a modern calculation method for the propagation of acoustic waves inside the airline is suggested. The solution for the flow field is provided by CFD solvers that produce solutions of the Navier–Stokes equations. A photon-based ray tracing technique is suggested as an acoustic analogy to simulate the propagation of the acoustic waves inside the same circuit and their interaction with the solid boundaries. The focus of this two-point design optimization process is to minimize the pressure loss inside the airline circuit at the same time it maximises the acoustic attenuation of the noise generated inside it, like that generated by the wind tunnel fan and heat exchanger.

The acoustics of the wind tunnel fan are optimized using the inverse cutoff design [3, 4]. The main purpose of this design is to minimize the broadband noise generated by the fan. To mitigate the higher harmonics of the blade passing frequency generated by the fan in the inverse cutoff design, a systematic evaluation of the impact of the most relevant fan parameters on the different noise contributions is performed. The impact is predicted using computational tools based on semi-analytical acoustic models. The prediction of noise is determined by semi-empirical scaling laws that describe the evolution of the sound pressure level of a noise source as a function of flow and geometry parameters. The changes in the aerodynamic performance introduced by those design modifications are verified with turbomachinery-oriented CFD solvers.

As far as the test section is concerned, several investigations have shown that it is not yet possible to reliably measure absolute noise pressure levels in closed test sections with hard walls. This is true for measurements of discrete tonal noise and broadband noise contributions alike. The best alternatives for producing quantitative acoustic results

Fig. 1 Sketch of a world-class aeroacoustic wind tunnel: Low speed wind tunnel Braunschweig (NWB) of the German–Dutch Wind Tunnels Foundation (DNW) (dark blue areas correspond to acoustically treated surfaces)
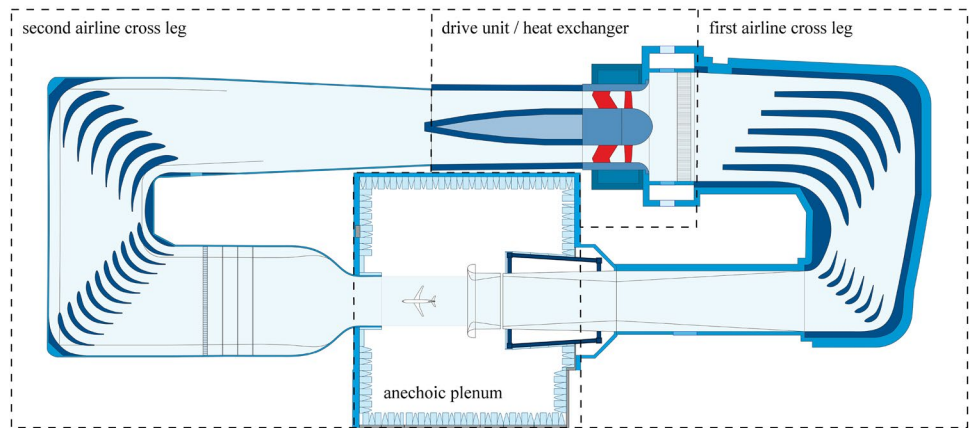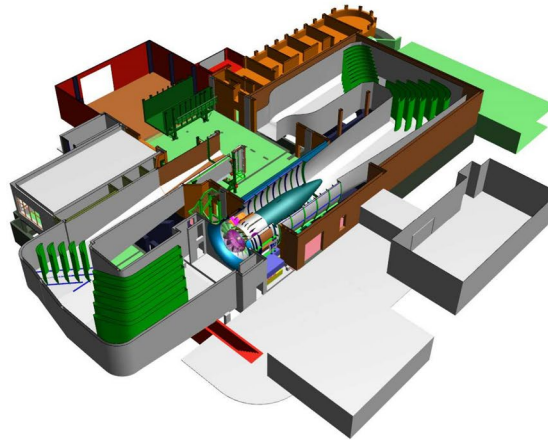
are still open-jet test sections and 3/4 open test sections surrounded by large anechoic plenums. The design and later assessment of the acoustic characteristics of the anechoic plenum is performed in both wind-off and wind-on conditions and makes use of room acoustics principles. Room acoustics is a subdiscipline of the acoustics branch that studies the sound behaviour in enclosed spaces, such as concert halls and recording studios, theatres, railway stations, and office buildings, to name a few. It is also known as architectural acoustics or building acoustics. The design aims to achieve two main objectives: to isolate the test section against external noise so that the resulting internal noise does not invalidate the measurements and to reproduce with high fidelity the acoustic free-field conditions for the acoustic measurements. Finally, the background noise and pressure fluctuation requirements in wind-on conditions are also discussed.

The final integration of the four sections into a complete aeroacoustic wind tunnel design is performed iteratively through the boundary conditions of the individual sections. Initially, a basic design of the four wind tunnel sections is completed separately based on preliminary macro flow field and acoustic assumptions. Then, in each iteration, the individual design of the sections is modified towards the optimum point and a new set of boundary conditions is calculated. These boundary conditions will be used as input in the subsequent iteration. The optimization process ends when both flow field and acoustic boundary conditions of all adjacent sections match and when all the global requirements of the aeroacoustic wind tunnel design are fulfilled.

2 Airline

The design of a wind tunnel airline with superior acoustic performance must be focused on the reduction of the flow-induced noise caused by high local flow velocities. Thus, as a first measure, the diffuser after the test section must be designed as large as possible to maximize the cross-section area of the wind tunnel at the location of both the first and second corners. Due to the stringent limitations on the maximum opening angle of a diffusor to avoid flow separation, this is normally achieved by installing a longer diffusor. The advantage of this design is twofold. First, it reduces the local flow velocity in the first and second corners and consequently the flow-induced noise produced by the flow

around the turning vanes. Furthermore, the turning vanes are located at a greater distance from the test section, which increases further the acoustic damping and decreases reflections between the vanes and the test section. Both effects increase the signal-to-noise ratio in the test section. Second, larger wind tunnel corners give more freedom to the design and optimization of the turning vanes without the penalty of higher pressure loss. In particular, it allows the turning vanes to be thicker and acoustically treated. This type of vane often has an aerodynamic shape and is made from perforated metal plates with back-filled glass wool used in typical sound absorbers. Figure 2 depicts the first cross leg of the same wind tunnel test case before and after the acoustic upgrade. Whereas the sketch on the left-hand side represents a pure aerodynamically designed airline, the one on the right-hand side shows a design optimization based on both aerodynamic and acoustic considerations. The figure clearly shows the size difference between the turning vanes of an aeroacoustic and a pure aerodynamic wind tunnel. In fact, the turning vanes in the second corner act as a bent splitter silencer and provide a counterpart to the annular acoustic muffler of the same length, situated downstream of the wind tunnel fan. In the example shown in Fig. 1, the acoustic muffler consists of an acoustically treated, very long fan tail cone surrounded by acoustically treated walls. This design is only possible after a substantial increase of the airline diameter. The figures suggest also that it is easier to implement acoustically treated turning vanes in large-scale wind tunnels than in smaller ones. The enlargement of the airline cross-section area near the second corner is also favourable for an optimized positioning of the heat exchanger (see Sect. 3).

The turning vanes contribute significantly to the acoustic characteristics of a wind tunnel. For that reason, their design must be carried out together with the design of the internal contour of the wind tunnel airline in such a way as to simultaneously maximize both the acoustic transmission loss through the airline and the aerodynamic characteristics of the tunnel. The latter means maintaining a high flow quality through the entire airline (regarding flow directivity, uniformity, separation, etc.), while minimizing the overall

pressure loss. A small pressure loss reduces the required power to drive the tunnel which in turn reduces the noise generated by the drive unit. The high acoustic transmission loss minimizes the noise produced inside the tunnel, in particular by the fan and the heat exchanger, to reach the test section.

The strong interaction between a solid structure with the flowing fluid in which it is immersed, as in the case of the turning vanes, or by which it is surrounded, as in the case of the wind tunnel inner walls, gives rise to a wide spectrum of multi-physical phenomena that results in a strong coupling between the aerodynamics and the acoustics. Therefore, the strategy to optimise only the acoustic properties of the airline by steering it using boundary conditions defined by aerodynamic considerations, or vice versa, does not lead to a global optimum. This constitutes a closed problem. The current contribution suggests an iterative optimisation of both objectives using high-fidelity CFD tools and a photon-based ray tracing technique for the acoustic layout. The optimization chain starts by generating the airline geometry based on the actual designing parameters. After a second step, in which the geometry is prepared and the numerical grid is generated, the calculation process is separated into two trails. The first one deals with the determination of the aerodynamic quality of the airline circuit. There is a strong aerodynamic and acoustic coupling between the turning vanes in the first and second corner of the airline because of the local low velocity of the flow and the short distance between them. To take this into account, the first and the second corner must be simulated together in the CFD and acoustic code as well. The same is applicable to the third and fourth corner of the wind tunnel airline. The second trail determines the acoustic quality of the airline circuit.

The evaluation of the aerodynamic quality is performed by a CFD solver. Based on the given geometry, which is discretized by a mesh, a flow solver produces a numerical solution of the averaged Navier–Stokes equations describing the flow physics. The numerical simulations are usually performed for a 2D cut of the airline to reduce the computational time. This simplification does not consider the

Fig. 2 Comparison between an aerodynamic optimized wind tunnel airline design (left) and a design optimized for both acoustic and aerodynamic applications (right) (for clarity, only the section of the airline located between the collector and the drive unit is represented)
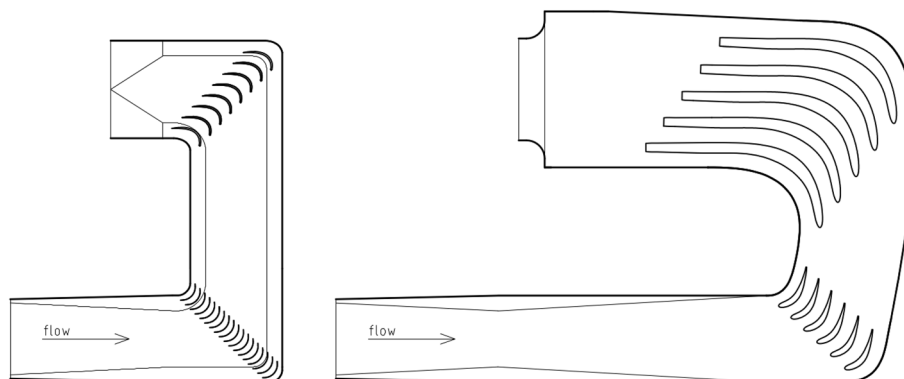
typical 3D boundary layer found in cascade flows. The aerodynamic objective is to minimize the pressure loss in the flow between the inlet and outlet section of the numerical domain. It is defined as follows:

$$\Delta p_{\text{loss}} = \frac{(p_{\text{tot}})_{\text{out}} - (p_{\text{tot}})_{\text{in}}}{\dot{m}}. \tag{1}$$

The total pressure loss and consequently the aerodynamic objective, must consider the mass flow rate because small changes in pressure loss are followed by changes in the mass flow through the simulation domain. This coupling effect is neutralized when introducing the mass flow rate into the equation, if a linear dependency between the total pressure loss and total mass flow is assumed. If compressibility effects are introduced through the Mach number, the total energy of the flow becomes the sum of the mechanical and the thermal energy components. In fact, it can be argued that the Mach number squared represents the ratio of the mechanical (kinetic) energy and the thermal component of the total energy. Following this path, the total pressure can be written as:

$$p_{\text{tot}} = p\left(1 + \frac{\kappa - 1}{2}Ma^2\right)^{\frac{\kappa}{\kappa-1}} \tag{2}$$

for the inlet and outlet sections of the numerical domain.

A light analogy is implemented to access the acoustic behaviour of the wind tunnel airline circuit including the turning vanes. Sound and light are in general of a different nature and perceived by two distinct senses [27, 28]. However, in terms of propagation and interaction with objects, they present some similarities. They both propagate as waves, sound waves being longitudinal waves of varying pressure. The propagation of light energy and its interaction with objects can be measured and described using techniques of radiometry from which global illumination models used in computer graphics are derived. There are two well-documented models [13, 28]: wave-based modelling and geometric modelling. The so-called wave-based modelling is based on the numerical solution of the wave equation, or Helmholtz–Kirchhoff equation. Therefore, it corresponds to a global illumination model. The numerical simulation based on this model provides very accurate results, but the complexity and the computation time increase drastically while increasing the highest frequency to be resolved [2].

The geometric modelling is a local illumination model. It is based on the calculation of the path of waves or particles through an environment with regions of varying propagation velocity, absorption characteristics and reflecting surfaces. This can be simulated with only a small amount of computational resources using a ray tracing technique. Ray tracing solves the problem by repeatedly emitting rays from a pixel into the scene, recursively generating reflected and refracted rays.

Both wave-based and geometric modelling can be mapped to the propagation of acoustic energy [7]. This implies that the propagation of sound waves can be simplified to a ray-based approach. For middle and higher frequencies, this assumption is true to a certain extent, because diffraction and interference processes are neglected. In contrast, wave-based effects become prominent at lower frequencies and ray-based methods can no longer be applied. The frequency range in which diffraction and other wave-based interferences are important is a function of several parameters. However, it is a common practice to define a limit based only on the comparison between the wavelength of the propagating wave and the size of the solid with which it interacts. Some authors state that the diffraction-free limit is lowered to the object of the size of the wavelength. Others require an order of magnitude difference between the wavelength and the size of the body before geometric optics could become useful. Bertram et al. [2] for example, define the lower frequency threshold for the applicability of ray tracing techniques as follows:

$$f = \frac{c}{\lambda} \approx \frac{c}{L}. \tag{3}$$

Using these criteria, the lowest frequency that can be simulated with the geometric modelling technique is approximately 100 Hz for a turning vane with an arc length equal to 3 m. For a mid-size aeroacoustic wind tunnel focused on tests with scaled models, this is a plausible vane size; the frequency value is about six times smaller than the lowest frequency of interest. Thus, the simulation of the transmission loss along the airline can be performed with a good degree of confidence with the geometric approach.

In conclusion, to determine the acoustic transmission loss in an aeroacoustic wind tunnel airline, a global illumination model is needed. Besides direct reflections of the sound waves on the turning vanes surface and internal walls, a significant amount of diffuse reflections takes place inside the tunnel airline. Ray tracing can only handle specular reflections, refractions and direct illumination (local illumination model). Effects such as caustics and indirect illumination (e.g., from diffuse reflections) cannot be computed, because it assumes perfect specular materials [13]. To take diffuse reflections into account, the ray tracing technique has been extended in recent years with Monte Carlo methods in which rays are distributed stochastically to account for all light paths. Another viable idea is to combine radiosity (wave-based modelling) with ray tracing into a hybrid technique. However, this technique needs a fine representation of the scene to render, which makes it very computationally demanding. A more modern approach makes use of a photon map. Photon mapping is a different approach than hybrid techniques [13, 14]. The idea is to change the representation

of the illumination. Instead of tightly coupling lighting information with the geometry, the information is stored in a separate independent data structure, a so-called photon map. The photon map is constructed from photons emitted from the light sources and traced through the domain. It contains information about all photon hits and this information can be used to efficiently render the object in a similar manner as radiosity is used in hybrid techniques. The decoupling of the photon map from the geometry is a significant advantage that both simplifies the representation and makes it possible to use the structure to represent lighting in very complex objects. The combination of photon mapping and Monte Carlo ray tracing-based rendering algorithms not only results in a more efficient algorithm but also represents a global illumination model.

The photon-based ray tracing techniques are normally applied to an airline in such a way that the physical boundary conditions of the numerical domain coincide with the geometry of the first or second cross leg of the wind tunnel. The inlet section of the domain is defined in the core of the airline circuit at the wind tunnel drive unit and the outlet section is defined close to the wind tunnel test section. The technique uses a planar light source at the inlet plane of the acoustic domain as a representation of the noise generated by the fan. In detail, a number of small, punctual light sources distributed over the plane are used to create a unidirectional source of light over the complete cross-section of the tunnel. This is comparable with the noise radiated by the fan into the airline. The interaction between light and the solid boundaries is characterized by the surface properties of the walls and by the type of reflection they generate. Thus, it must be distinguished between hard-walled and soft-walled surfaces. A hard-walled surface means the complete sound energy is reflected and nothing is absorbed. With a soft-walled surface, part of the sound energy is dissipated into heat in the material and therefore the reflected sound wave is weakened. Further on, depending on the surface of the wall, there are two kinds of reflections: specular and diffuse reflections. Specular reflection is the light reflected from a smooth surface at a definite angle. Diffuse reflection is the reflection of light such that the incident ray on the surface is scattered at all directions. In the end, the different reflection mechanisms are considered by the acoustic ray tracing approach using two parameters: the fraction of soft- and hard-walled surface and fraction of diffuse and specular reflection. For acoustically treated walls, like turning vanes made from perforated metal plates with back-filled glass wool, it is a non-trivial task to determine both values.

The acoustic quality of the actual configuration is a function of the brightness of the image constructed in the outlet plane of the acoustic domain. For the same inlet light source intensity, a less bright image at the outlet of the acoustic domain means a higher acoustic transition loss through the

airline and consequently a better acoustic quality. To keep the method simple, the image plane is discretized by N monitoring points, or microphones in the acoustic analogy. The brightness histograms of all microphone positions are typically calculated. This histogram reflects the distribution of the n brightness levels of a picture. For each microphone position, the overall brightness is calculated based on the logarithmic sum assuming incoherent sound sources using the following equation:

$$L_{\mathrm{m}i} = 10 \log \sum_{j=1}^{n} 10^{\frac{h_j}{10}}. \tag{4}$$

This value, in the acoustic analogy, represents the sound pressure level measured by each microphone. The logarithmic summation takes into account the physical effect that the sound sources with the highest levels make a bigger contribution to the overall sound pressure level. In the end, the overall sound pressure level is computed adding the contribution of all N microphones again using the logarithmic summation as follows:

$$L_{\mathrm{p}} \equiv L_{\mathrm{m}} = 10 \log \sum_{i=1}^{N} 10^{\frac{L_{\mathrm{m}i}}{10}}. \tag{5}$$

This value defines the acoustic objective. At the end of both trails, the aerodynamic and acoustic results for the current geometry are known as numerical values and constitute a design point. After that, a new set of designing parameters is generated and a new calculation run is started.

Figure 3 shows a typical two-point design optimization map for an airline design of an aeroacoustic wind tunnel.
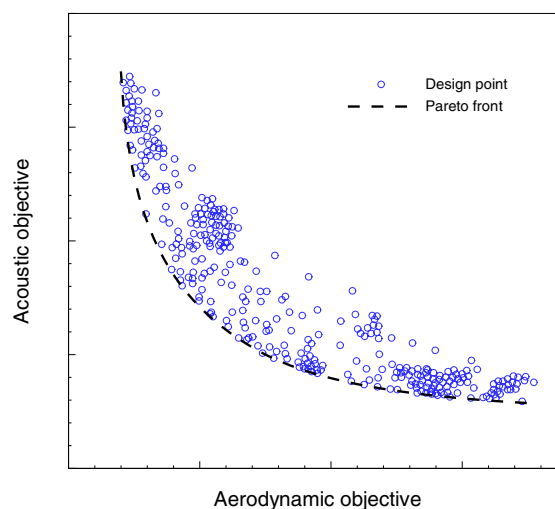

Fig. 3 Typical two-point design optimization map for an aeroacoustic wind tunnel airline design

The result of each calculation run is represented by a circle in the plot. The horizontal axis represents the aerodynamic objective. A lower aerodynamic objective is associated with a smaller pressure loss and represents a better aerodynamic quality of the airline. The acoustic objective is shown on the vertical line. As for the aerodynamics, the lower the acoustic objective the higher the acoustic quality of the airline. It means a higher acoustic damping through the airline legs and better absorption of the internal noises generated in the wind tunnel. The two-point design optimization map is followed by the determination of the Pareto front, or optimization line. Figure 3 also highlights the strong dependent and competitive character of an aeroacoustic design. Improvements on the acoustic properties of a wind tunnel airline are associated with a reduction of the aerodynamic qualities and vice versa. This is especially valid for mid-size and small wind tunnels, because the thickness of the turning vanes cannot be scaled. The final design point of the airline is found along the Pareto front and should correspond to the best compromise solution that fulfils the global aerodynamic and acoustic requirements of the aeroacoustic wind tunnel design. It should also fit the design of the other wind tunnel sections. A good example of this dependency is the interaction between the airline design and the design of the wind tunnel drive unit. If fan power is a capital design constraint, the final airline design point must prioritise the aerodynamic objective with a penalty to the acoustic quality of the aeroacoustic wind tunnel. The final design point moves accordingly to the left along the Pareto front. In opposition, the final design point can be moved to the right along the Pareto front if the available power in the fan allows for a slight increase of the pressure loss in the airline of the wind tunnel. This way, the acoustic characteristics of the wind tunnel airline can be maximized. An example of the application of the method suggested in the present test is described in Ref. [16].
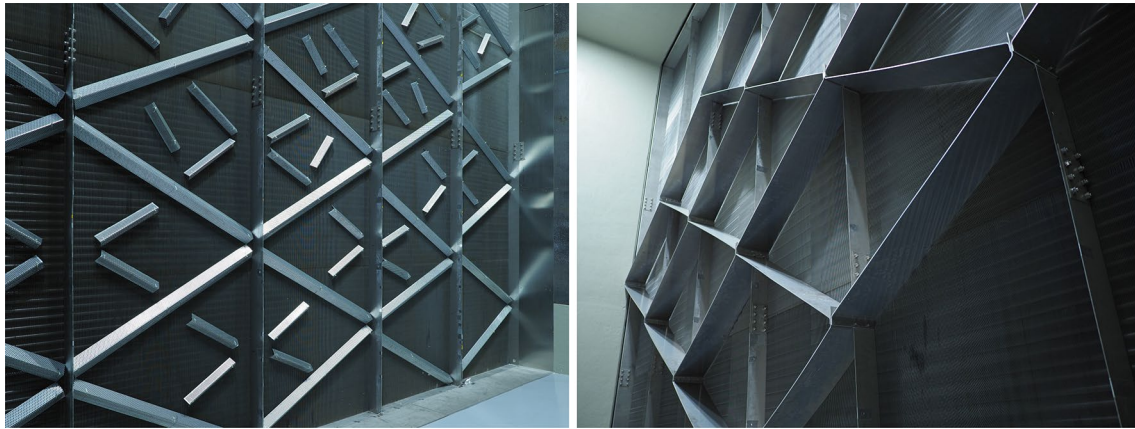
3 Heat exchanger

Because of their singular geometry and mechanical characteristics, tubes in heat exchangers are prone to experience fluid-elastic instabilities and/or fluid–acoustic coupling effects [21]. Whenever this is observed, the heat exchanger can be improved to reduce the self-generated noise at the source. Among all flow-induced sound interaction mechanisms, the so-called Parker resonance is a common one [23, 24, 36]. This interaction mechanism is commonly found in gas heat exchangers in power plants [8] and in axial-flow fans [34]. It describes the flow-excited resonant sound generation in cascades of flat plates in a rectangular duct, as the vortex shedding frequency from the trailing edge of the plates approaches the frequency of an acoustic transversal

mode of the duct. When it manifests, tonal noise arises at the resonance frequencies.

Any heat exchanger also introduces a significant pressure loss in the airline of the wind tunnel. For this reason, it is often located in the settling chamber to take advantage of the large cross-section area and low flow velocity in this part of the wind tunnel, despite the decrease in cooling efficiency while reducing the flow velocity. Therefore, an acoustic interaction between the heat exchanger and the other components that are in a settling chamber, such as the flow straightener and screens, must be expected and considered along with the self-generated heat exchanger noise. Both experimental tests and in situ inflow measurements have shown that the sound pressure level created by the flow through the combined heat exchanger, flow straightener and screens is significantly higher than the noise radiated by the flow passing through the individual elements [12]. Depending on the frequency range, the sound pressure level due to interaction effects can be 10 dB greater, or more, than the sound pressure level generated in the screens alone. Due to the proximity of these components to the test section, the negative acoustic consequences that arise from the interaction between the heat exchanger, flow straightener and screens have a direct and relevant impact on the background noise. The same studies also concluded that the combined heat exchanger and flow straightener is primarily responsible for the background noise spectrum in the mid- to high-frequency range (3 kHz to above 10 kHz). Additionally, some tonal noise components were registered at low flow velocities.

To minimize this problem, the heat exchanger, which in a classic aerodynamic wind tunnel is usually placed in the settling chamber, must be repositioned in an upstream location, ideally near the drive unit and far away from the test section. To achieve this, the cross-section area of the wind tunnel airline in between the second corner and drive unit fan must be of similar size as the settling chamber. With this design, the heat exchanger is placed close to the noisiest element of the entire wind tunnel so the acoustic penalty it introduces is minimal. Additionally, all acoustic measures introduced in the flow path inside the airline, such as the annular muffler installed downstream of the fan and splitter attenuators, will constitute a damping barrier for the propagation of the noise generated by the drive unit and heat exchanger alike.

To inhibit the self-generated noise and any acoustic resonance triggering mechanism in the heat exchanger tubes, either the periodic vortex shedding or the synchronization with an acoustic mode must be disrupted, or both simultaneously. This is the reason why the heat exchangers of some aeroacoustic wind tunnels are installed with baffles in the upstream side (see Fig. 4). These elements, generally located in a random arrangement, significantly increase the unsteadiness and the turbulence intensity of the flow

Fig. 4 Baffles (left) and acoustic partitions (right) installed in the heat exchanger of DNW-NWB

upstream from the tubes that constitute the heat exchanger. As a direct consequence of the new upstream flow condition, the wake flow created by the tubes is significantly smaller and weaker as is the coherence of the vortex shedding developed behind them. An alternative solution to the baffles is to manufacture the heat exchanger with tubes mounted with tripping elements or with dimple structures on their surfaces. Both solutions will force the flow boundary layer on the surface of the tubes to become turbulent with similar effects to the vortex shedding developed behind them. Figure 4 also shows the section of the airline immediately after the heat exchanger, divided into small, irregular partitions. In opposition to the baffles, this solution acts on the fluid–acoustic rather than fluid–structure interaction mechanisms. The flow partitions have the property to disrupt the mechanism of energy transfer transversal to the flow. More importantly, the irregular partitions breakdown the acoustic transversal resonance mode of the duct, proportional to its diameter or width, into a wider range of smaller wave lengths. As soon as the principal acoustic transversal resonance modes of the duct are not restricted to a single wave length or frequency and its higher harmonics, the transversal standing waves that will be triggered perpendicular to the flow will be out of phase and will destructively interfere with each other. This mechanism will prevent the amplification through resonance of an acoustic transversal standing wave across the airline cross-section downstream of the heat exchanger.

4 Collector

Various types of collectors have been tried in both aerodynamic and acoustic wind tunnels. However, just two of these types have been selected as a standard solution in modern wind tunnel designs.

The funnel collector has its name attributed to its funnel-shaped geometry. The collectors of this type are commonly made of straight walls and are designed to ingest the free flow together with its shear layer. As a result of different entrainment mechanisms, the diameter of the free flow increases in the stream-wise direction along the test section. Because the mass flow must remain constant in the airline circuit, part of the flow that enters the funnel is deflected backwards close to the funnel walls and is forced to flow out of the collector. This implies that the flow stagnation line, i.e., the line at the surface of the collector where the fluid is brought to rest, is located at some point inside the collector. If the inlet cross-section area of the funnel collector to cross-section area of the contraction ratio is small, undesired fluid–acoustic coupling effects arise as the flow stagnation line moves close to the leading edge of the collector walls. For this reason, funnel collectors are only effective if their cross-section area is considerably bigger than that of the contraction. In addition to the large space they occupy, funnel collectors also present an aerodynamic drawback. The flow experiences a strong deceleration in front of this type of collector, because of its larger diameter compared with the contraction area. Consequently, the static pressure rises in the stream-wise direction and its distribution can no longer be considered constant along the test section.

The disadvantages of the funnel collectors are counterbalanced by their superior acoustic quality when installed with the appropriate acoustic lining. Because of their size and simple geometry, the collectors can be made with sound-absorbing walls and/or covered with pile fabrics. The acoustic advantage is a consequence of the fact that the entire shear layer flow interacts directly with an acoustically treated surface. Moreover, funnel collectors are not installed with a breather gap between the collector and the diffusor which can be a relevant noise source in the test section. For these reasons, this type of collector is preferable for pure acoustic

wind tunnels with the penalty of a minor degradation of the aerodynamic quality of the flow.

Wing collectors, or the so-called Prandtl rings, are wing-shaped deflectors that are mounted upstream of the diffusor such that a breather gap is created between the collector and the diffusor. In this design, the shape of the collector walls is optimized so that the flow stagnation line coincides with the leading edge of the collector. This way, the additional mass flow that results from the jet growth in the test section is not reverted inside the collector walls but is forced to flow out of the collector through the breather gap. This gap and the flow it generates constitutes a significant noise source in the test section especially when it is hit by vortices in the flow. The acoustic treatment of this type of collector is more challenging because of their smaller size and highly aerodynamic shape. In most of the cases, flocked or pile fabrics are used as wall material for the collector surface to reduce the noise generation (see discussion on pile fabrics in Sect. 7).

The advantage of the wing collectors is that their geometry can be optimized to impose a minimum deceleration in the flow. Consequently, the static pressure increase in front of the collector can be mitigated. Additionally, the collector to contraction cross-section area ratio can be minimized resulting in small collectors. Thus, the complete length of the test section can be also minimized which is advantageous for the overall energetic balance of the wind tunnel. Because of this, wing collectors are the most appropriate choice for aerodynamic wind tunnels.

Despite the numerous attempts to solve this problem by means of CFD optimization algorithms, an established method to design an aerodynamically optimized collector that is at the same time acoustically very quiet has not yet been found. The collectors that are installed in the most modern aeroacoustic wind tunnels were designed almost by trial and error using a numerical, iterative approach similar to that suggested for the design of the turning vanes inside the wind tunnel airline. Thus, the results from this approach were specific for each particular wind tunnel and have not yet led to an optimized type of collector to be implemented as standard in all aeroacoustic wind tunnels to come.

5 Buffeting suppression mechanisms

Another aspect which deserves special attention during the design of an acoustic wind tunnel is the low-frequency fluctuations in pressure and velocity that are prone to appear at distinct ranges of flow velocity in many open test sections. The large-scale vortices shed from the trailing edges of the wind tunnel contraction, combined with the development of shear layers between the wind tunnel core flow and the quasi-quiescent surrounding region, provide a source of flow unsteadiness that can couple with various fluid–structure–acoustic interaction mechanisms in the wind tunnel. The wind tunnel pulsations they generate, also known as wind tunnel pumping or buffeting, have a negative impact in the aerodynamic quality of the flow and thus in the quality of the measured data [37]. As far as acoustics is concerned, wind tunnel pulsations not only increase the background sound pressure level within the low-frequency range but also distort the acoustic measurements, because the noise generated by the flow around the test model is modulated at the frequency of the pulsations. The physical mechanisms of the amplification of low-frequency pressure fluctuations in open test sections and their suppression have been the subject of a variety of investigations and proposals to solve the problem. From a purely aerodynamic point of view, the most widely used method are vanes, tabs and teeth (Seiferth flaps) that protrude into the flow at the contraction exit [15, 22, 30]. However, these vortex generators produce high-frequency, broadband flow noise right in the inlet of the test section and thus are generally considered unacceptable for most aeroacoustic wind tunnel applications [25].

More complex alternatives for the attenuation of the pressure fluctuations comprehend both active and passive suppression methods. Active resonance control (ARC) systems essentially consist of a microphone to measure the pressure fluctuations in the wind tunnel anechoic plenum and a large speaker driver system to pump sound waves inside the airline circuit. A phase delay is introduced between the microphone signal and the speaker output to generate anti-phase sound levels at the resonance frequencies inside the airline to cancel the pressure fluctuations. This system has proved to be very efficient in eliminating the periodic velocity fluctuations in small wind tunnels and does not introduce additional noise into the wind tunnel. In actual cases where systems of this kind were applied, reductions of pressure fluctuations of up to 20 dB were registered [37]. However, the high price and complex operation associated with ARC systems tend to define them as not cost effective.

As far as passive methods are concerned, Helmholtz resonators can be implemented to remove the pressure fluctuations that occur at distinct frequencies [35]. The physical characteristic of a Helmholtz resonator consists of a large volume communicating with the airline circuit through a short duct. The main acoustic characteristic of a Helmholtz resonator is the ability to be tuned to a single frequency. The resonance frequency of a single resonator is defined as:

$$f = \frac{c}{2\pi}\sqrt{\frac{A}{l_{\mathrm{ef}}V}}, \tag{6}$$

where V is the fluid volume, A is the duct cross-section area and l_{ef} is the duct effective length. The latter is given by

$$l_{ef} = l + \delta, \tag{7}$$

where l is the duct length and $\delta = 0.85d$, where d is the duct diameter.

The absorption capability of the Helmholtz resonator can be understood as follows: the air in the communicating duct oscillates back and forward as a single mass and the large volume acts as a spring or restoring force. Friction resistance is encountered by the alternating fluid inside and around the communicating duct. Hence, acoustic energy is absorbed, mainly in the region around the resonance frequency. The larger the mass flow, the larger the damping effect of the resonator. The Helmholtz resonator is an efficient method of mitigation of the low-frequency fluctuations inside the wind tunnel but at the expense of being effective for only a short frequency range around the resonating frequency. Multiple resonator volumes are needed to broaden the frequency range of the absorber. In addition, it normally requires large volumes relative to airline volume to be truly effective at very low frequencies.

Another passive method of attenuation of pressure fluctuations is the implementation of a sudden contraction in the cross-section area of the airline circuit. With a sophisticated design, a sudden contraction originates an impedance mismatch inside the wind tunnel airline that is capable of providing a strong absorption of pressure fluctuations in the low-frequency regime. It is not yet completely understood what the real interaction mechanisms between the airline discontinuity and the low-pressure waves are. Preliminary tests tend to prove that the impedance mismatch method constitutes a very efficient method of suppression of the low-frequency pressure fluctuations inside the airline for a wide range of flow velocities. In addition, it does not show the major penalties that are characteristic of the other methods. The shape of the contraction should be chosen to create a sudden increase of the flow velocity with a minimum penalty on the local pressure loss in the airline circuit (for example, using sudden contractions with rounded corners). An example of a sudden contraction is shown in Fig. 1. It is located after the second corner of the wind tunnel, in between the heat exchanger and the fan. In this design, the sudden contraction was also used to adapt the large cross-section area of the airline after the second corner to the narrower diameter of the fan.

6 Drive unit

The wind tunnel fan is certainly one of the few components of a wind tunnel that can be independently improved to reduce noise emission at the source. The main objective of the acoustic optimization is the reduction of broadband noise while keeping the tonal noise at a low level and the aerodynamic performance unchanged.

The fan is known for generating different types of noise that arise from all sorts of mechanisms of noise generation. The most relevant include rotor blade and stator vane trailing edge noise, rotor– and stator–inflow–turbulence interaction noise, and rotor–stator interaction noise. Apart from the harmonic tonal contribution of the rotor–stator interaction, all other noise sources are broadband in nature. Among these, the inflow turbulence-induced noise is normally predicted to play a role in the lowest frequency range, while rotor blade trailing edge noise is expected to be dominant at higher frequencies. As far as peak frequencies are concerned, the peaks of the broadband contributions are determined by the relative flow velocity and turbulence length scale, whereas the peak frequencies of the tonal noise are centred on the blade passing frequency and its harmonics.

The impact of the fan design modifications on the different noise levels of a ventilator or an aero-engine fan is commonly predicted by means of computational tools based on semi-analytical acoustic models. The prediction of noise is given by semi-empirical scaling laws that describe the evolution of the sound pressure level of a noise source as a function of flow and geometry parameters. The aerodynamic impact of those design modifications is later verified using turbomachinery-oriented CFD solvers. Examples of both acoustic and aerodynamic solvers for fan applications can be found elsewhere [1, 10, 17, 18, 33]. This approach allows for only the prediction of trends. Otherwise, it requires complicated calibration methods for producing results on the absolute sound pressure levels.

Recent developments have led to a fully analytical formulation of the noise generation without the necessity of calibrating the models to predict absolute levels [19]. With these improvements, it is possible to compare and superimpose the absolute sound pressure level produced by several noise sources. This is very useful when the turbomachinery design is supported by an automatic multi-object optimisation process. No matter the prediction method, the acoustic design procedure must be based on the variation of noise relevant parameters and systematic evaluation of their impact on the different noise contributions. The most relevant parameters are: blade count of the rotor and stator, rotor velocity, axial distance between rotor and stator, sweep angle of the stator vanes, and inflow turbulence.

Figure 5 shows the results of the fundamental contribution of the blade passing frequency and also the first three harmonic components as a function of the rotor and stator blade count obtained after the simulation of a typical wind tunnel fan. The impact of the blade count on the broadband noise for the same fan is presented in Fig. 6. Two regions presenting a cutoff design can be identified in Fig. 5 (1-BPF). The triangular domain in the upper right-hand corner of the scalar map corresponds to the standard cutoff design in which the number of stator vanes is higher than
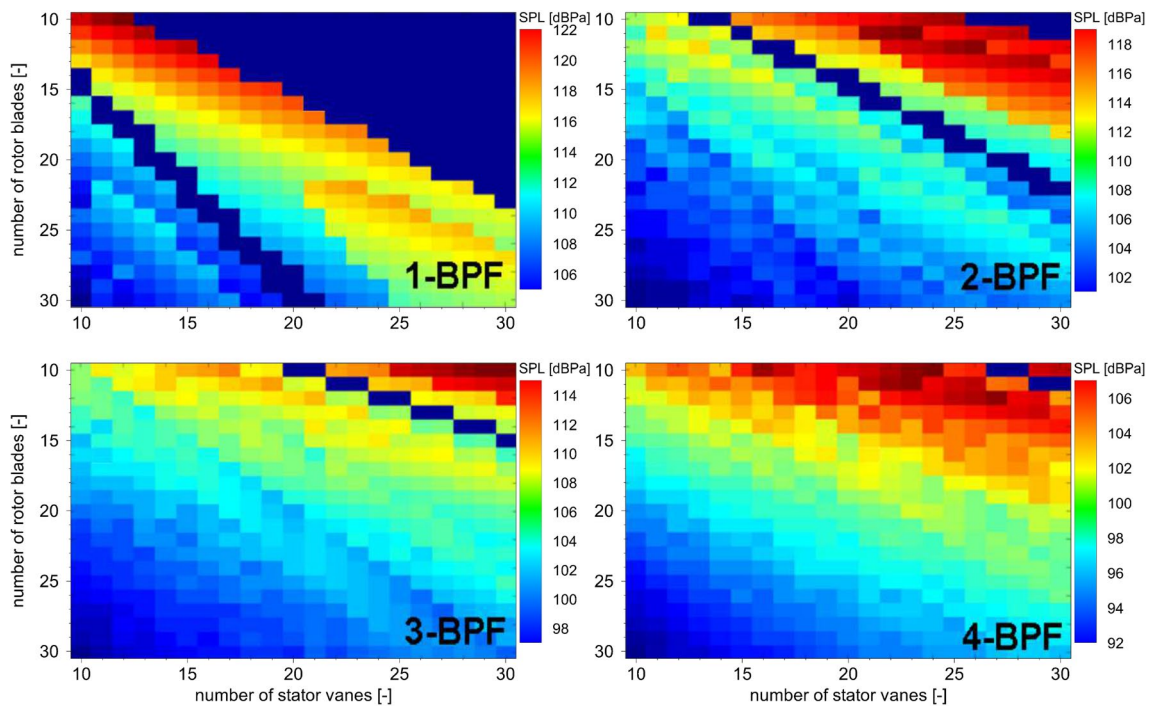
Fig. 5 Tonal sound pressure level of a typical wind tunnel fan as a function of both rotor and stator blade count for the first four blade passing frequencies
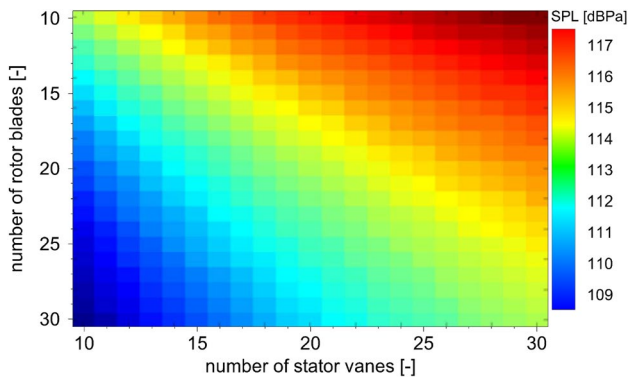
Fig. 6 Broadband sound pressure level of a typical wind tunnel fan as a function of both rotor and stator blade count

the number of rotor blades. Classic aerodynamic wind tunnel fans often utilize this design. It is optimized for tonal noise cancellation, since the first harmonics of the blade passing frequency of the rotor–stator interaction are non-propagated.

For acoustically optimized fans, it is advantageous to apply the so-called inverse cutoff design. This design makes use of a lower stator to rotor blade count ratio and its domain is restricted to a diagonal line in Fig. 5 (1-BPF). In this line, the number of stator vanes is smaller than the number of rotor blades. The new design is selected to reduce primarily the broadband noise through the lower count of stator vanes.

Broadband rotor–stator interaction noise increases proportionally with the number of sound emitters, in this case the stator vanes. Furthermore, broadband rotor–stator interaction noise is proportional to the integral turbulence length scale in the rotor wake. With the latter being proportional to the pitch, it is coherent to expect the broadband rotor–stator interaction noise to decrease while increasing the number of rotor blades. The combined effect of these two tendencies is shown in Fig. 6.

Both broadband noise-generating mechanisms, rotor–stator and stator–inflow–turbulence interaction noise, are proportional to the number of stator vanes. Similarly, rotor–inflow–turbulence broadband interaction noise is proportional to the number of rotor blades. Consequently, and from an acoustic point of view, a small number of rotor blades are more suitable in the event of high incoming flow turbulence.

The solidity of the blades in both the stator and rotor is a very important aerodynamic parameter and directly affects the pressure rise of the fan. To maintain the aerodynamic characteristics of the fan unchanged, the number of blades must be changed while keeping the blade solidity constant. This means to adjust the blade chord as a function of the number of blades. This design constrain has a direct impact on the trailing edge noise, because it does not depend on the blade count at constant solidity. For this reason, no trailing edge noise variations are expected for the rotor and stator.

However, the inverse cutoff design has an acoustic penalty. While the standard cutoff design can be extended to the higher harmonic components of the blade passing frequency, no such opportunity is given by the inverse cutoff design method, because only the fundamental frequency is cutoff (see Fig. 5). Therefore, it is safe to expect higher tone levels with the inverse design, since the second harmonic of the blade passing frequency (and higher) can propagate inside the tunnel airline. To counterbalance the higher tonal contributions of the fan-generated noise, the axial distance between the rotor and stator and also the sweep angle of the stator vanes can be increased.

Variations of the axial distance between the rotor and stator have no influence on the aerodynamic performance of the fan. This is true to a certain extent. From an acoustic point of view, both rotor–stator broadband and tonal noise contributions decreased while increasing the separation between the two blade rows. The noise reduction is due to the decay of the turbulence intensity as the wakes after the rotor are convected downstream. Actually, this trend should be even more pronounced for the tonal contributions, because interference effects contribute to the noise reduction as well as the wake decay. The radial phase shift of the incoming wakes (source excitation) is amplified by the inter-stage swirl as the wakes develop downstream. Due to this phase shift, the leading edges are excited at different instants along the span, which induces noise cancellations. It should be emphasised the rotor–stator separation must be bigger if the number of blades is reduced, because with fewer blades the decay of the potential field is slower and therefore needs a larger distance to decrease by the same amount as with the original design.

As a rule of thumb, the most efficient distance between the two blade rows is about one blade chord spacing. For larger distances, the decay of turbulence is slower and reaches the point where the acoustic benefit is too small when compared with the aerodynamic penalty due to the increase of the pressure loss. Trailing edge noise and inflow turbulence interaction noise due to the ingested turbulence are unchanged, because those sources should be independent from the separation distance between the blade rows.

The introduction of a sweep angle on the stator vanes is proposed mainly to reduce the tonal contribution of the noise produced by the periodical impingement of the rotor wakes on the stator vanes [9, 38]. The principal mechanism responsible for the noise reduction is the radial phase shift introduced by the tilted wakes as explained by Envia [9]. This effect can be strongly amplified by introducing a sweep [11]. Presumably, the sweep also has an effect on the source strength due to the change in the inclination of the leading edge relative to the mean velocity and the lengthening of the span. This means a reduction of the relative velocity in the case of swept stator, which usually induces a noise reduction despite the lengthening of the leading edge. Combined with the effect on correlation, this could explain why broadband noise is also reduced by choosing a swept stator [39]. However, special attention must be given to the sweep angle of the stator vanes close to the wind tunnel wall, because they can increase the local pressure loss significantly. To keep this effect bounded, it is interesting to investigate V-shaped or interrupted sweep vanes. The acoustic efficiency of these types of vanes is expected to be slightly lower than the original sweep vanes. Thus, the design must achieve a compromise between acoustic and aerodynamic quality. Several experiments have already shown that stopping the sweep angle at approximately 85% of the blade span leads to a significate acoustic gain with very limited aerodynamic penalty compared to a radial stator.

Comparing all advantages and disadvantages of the acoustic design of a wind tunnel fan, it can be shown that the configurations with a small number of stator vanes and a larger number of rotor blades are more beneficial. This is true assuming the incoming flow turbulence intensity is not too high and the tonal noise associated with the higher harmonic components of the blade passing frequency is mitigated by an optimized geometric definition of the rotor and stator blades.

Finally, one should account for the effects of the velocity of the rotor. It is easy to assume that this parameter has great importance because the sound pressure level generated by a blade increases roughly with the 5th power of the flow velocity measured in the relative frame of reference. Rotor blade trailing edge noise, rotor–inflow–turbulence interaction noise, and rotor–stator interaction noise decreased while reducing the rotor velocity at constant fan pressure differential. This noise reduction is a direct consequence of the reduction of the local flow velocity. In this case, the solidity must increase to compensate for the velocity reduction, which means an increase of the chord length. Stator–inflow–turbulence interaction broadband noise slightly increases due to the increase of the relative flow velocity at the stator vanes' leading edge, whereas stator trailing edge broadband noise remains almost constant. The rotor velocity reduction is directly associated with the optimization of the wind tunnel internal pressure loss and to the early design considerations of the drive unit. Reducing the rotor velocity is not only beneficial for supersonic rotors (for which the suppression of shock-induced buzz-saw noise is a well-known technique) but also for low-speed rotors. The maximum velocity reduction at constant fan pressure rise is limited by the technological advances in aerodynamic design and represents one of the major challenges for designing both quiet and efficient wind tunnel fans.

7 Anechoic plenum

Acoustic measurements should be performed in a fully anechoic, or at least semi-anechoic, environment to provide reliable results of the strength and directivity of an acoustic noise source. Such an environment is reproduced with sound-absorbing materials, often in special shapes, which efficiently suppress the reflections of acoustic waves on the solid walls of the test section. In such an environment, the noise source can be investigated in quasi-free-field conditions. But most actual wind tunnel facilities make use of closed test sections with hard walls for aerodynamic investigations. To provide well-defined boundary conditions, the test section walls are made as flat as possible and from solid materials, like metal or glass for optical access to the inside of the test section. Acoustically, these hard and flat walls act as efficient reflecting surfaces for sound waves.

To gain insight on the impact of the interference effects created by hard-walled test sections in the acoustic measurements, DNW investigated the standard closed test section of the DNW-LLF. This standard test section has a width of 8 m, a height of 6 m and an overall length of 20 m. The tests were carried out in both wind-off and wind-on conditions with one traversing and several stationary inflow microphones to cover the entire area of the test section. All microphones were installed at a height of about 1.5 m above the test section floor with aerodynamic forebodies, also known as nose cones. During the investigation in wind-off conditions, a loudspeaker was used to generate tonal noise signals at the typical position of the test model. Sinusoidal signals between a few hundred and several thousand Hertz were tested. The results showed a complex pattern of interferences for the local sound pressure level as a function of both the axial and lateral position in the test section. Within a distance variation of a few centimetres in the position of the traversing microphone, the local sound pressure level could change up to more than 20 dB. When repeating the tests with a white noise signal, fluctuations of the overall sound pressure level were still observable but significantly smaller and limited to several dB. The investigations in wind-on conditions were concentrated on the characteristic tonal noise of the wind tunnel fan. These tones were clearly observed in all acoustic spectra with a typical distance to the broadband noise level of 10 dB and more. During measurements at different flow velocities, a clear correlation between the measured sound pressure levels and the required electric power to operate the wind tunnel fan was not registered. A low reproducibility between different test configurations was also observed. For the flow velocity range of the tests, the sound pressure level variations between adjacent microphones or between different measurement runs were observed at up to 10 dB.

The discrepancy observed in the results of the local sound pressure level can only be attributed to the complex acoustic interference pattern inside the closed test section created by multiple reflections on the hard walls. Small flow velocity variations modify the local interference pattern due to convection effects, which produces a similar effect to changing the position of the traversing microphone inside the test section. In a similar way, small mechanical changes in the test setup are capable of changing the interference pattern for tonal noise signals. For broadband noise contributions, like the wind tunnel background and model airframe noise, smaller differences between the sound pressure levels measured by adjacent microphones were registered. In general, the results from different test setups and runs also showed a much better agreement compared with those obtained with tonal noise signals.

Further investigations involving noise measurements in closed test sections with microphones placed outside of the flow, like inside the cabin of a passenger car in the test section, provided similar conclusions. In this case, the effects of reflections on the car were added to the reflections on the hard walls of the test section. Once again, the measured sound pressure level of tonal signals was much more unreliable compared to broadband noise contributions.

Based on these investigations, it can be said that it is very difficult to reliably measure absolute sound pressure levels inside closed test sections with hard walls with the classic inflow free-field microphone technique. Even delta measurements do not provide reliable results for the sound pressure level comparison between two test configurations. For measurements of broadband noise contributions, the scenario is slightly better but still not acceptable for quantitative analysis.

Differently, noise mapping techniques have been successfully applied in closed test section environments, in special high order deconvolution methods such as CLEAN-SC [31] or, more recently, high-resolution CLEAN-SC [32]. These deconvolution methods have proven to be significantly more reliable than the conventional beamforming technique in reverberant, noisier environments. The noise mapping techniques make use of phased microphone arrays to detect the spatial distribution of sound sources. The array microphones are often flush mounted in the walls of the test section and therefore directly exposed to the boundary layer that developed along them. As long as the size of the test section is big enough compared with the dimensions of the model and the acoustic wave length of interest, wall-mounted phased microphones arrays are significantly less sensitive to interference effects caused by the hard walls.

In recent years, tests have been performed in closed test sections with acoustic absorbing walls, like perforated walls

with a sufficiently thick layer of acoustic material behind them, or acoustically semi-transparent walls, like walls made from thin Kevlar fabric [5, 6, 26]. In both cases, the reflected acoustic waves on the inner walls of the test section are minimized. However, these new types of walls have their own problems when it comes to defining the aerodynamic boundary conditions inside the test section accurately, and they have not yet proven their efficiency.

The best acoustic alternatives to closed test sections are the open-jet and 3/4 open test sections surrounded by a large acoustic plenum with all walls covered with acoustic lining. Most modern aeroacoustic wind tunnels offer such kind of test sections for acoustic tests [12]. They provide an anechoic environment for the measurements and the possibility to reliably measure absolute noise pressure levels. Because the microphones can be placed outside of the flow at a bigger distance from the test model, the acoustic far field can also be evaluated correctly. The biggest drawback imposed by open test sections to acoustic measurements is associated with the fact that the sound waves emitted by the test model must propagate through the free flow shear layer before reaching the microphones. The propagation of the sound waves through the shear layer causes refraction, spectral broadening and loss of coherence between the signals arriving at different microphones. The latter affects mostly the results of the noise mapping techniques. These effects depend on the Mach number of the flow, both noise source and microphone position relative to the shear layer, and sound frequency. Because they increase while increasing the frequency of the propagating sound, the maximum sound frequency that can be measured in an open test section with acoustic plenum is limited. This can cause problems in measuring the noise generated by small-scale models.

The installation of a fully anechoic or a semi-anechoic plenum around the wind tunnel test section serves a twofold objective. First, to isolate the test section and consequently the acoustic experimental setup against external noise, so the resulting internal noise does not overrule the measurements. Second, to reproduce with high fidelity the acoustic free-field conditions inside the test section. This may require the use of single- or double-wall construction with proper vibration isolation to reduce air- and structure-borne noise transmission. At the same time, the volume of the anechoic plenum must be as big as possible. The noise pressure level decays with the square of the distance. Consequently, the amplitude of the sound pressure waves reaching the walls of the plenum is smaller in large facilities. Additionally, any pressure fluctuation and/or secondary flow that might occur inside the anechoic plenum have less interaction with the plenum walls. In practice, the dimensions of the plenum are limited by the host wind tunnel building infrastructure and by construction and maintenance costs. For the same reasons, large anechoic plenums are usually constructed in

the shape of a rectangular cuboid. Even though this design is prone to developing standing waves, the fundamental frequency of resonance is usually low enough to be disregarded. In the case of smaller plenums, this effect should not be neglected and non-regular shapes should be considered.

Figure 7 shows an example of an aeroacoustic wind tunnel anechoic plenum. It has a cross-section area equal to 16.4 m × 7.8 m (the cross-section area of the contraction is equal to 3.25 m × 2.8 m) and it is symmetrically mounted with respect to the wind tunnel axis. The length of the anechoic plenum is equal to 14.2 m, about 2.4 times the length of the wind tunnel test section. Acoustic lining made from sound-absorbing material shaped into wedges, such as those shown in the figure, is a well-proven method to optimise the acoustic damping and to achieve a free-field environment inside the anechoic plenum. The wedge-shaped geometry ensures a gradual change in the acoustic impedance of the transmission media, ensuring that sound waves are absorbed by the material, rather than reflected at the interface. In choosing the dimensions and material of the acoustic lining, the most important decision point is the frequency range in which the anechoic plenum must be effective. For the most aeronautical acoustic problems, the sound frequency range below 4 kHz is of special interest. Because of the specific aerodynamic problems found in road vehicles, this value is even smaller for automotive tests. Thus, wind tunnels that focused on full-scale models have anechoic plenums generally designed to operate effectively in the frequency range from about 100 Hz up to 4 kHz. In smaller wind tunnels, where test models are scaled down relative to their full size, the frequency range of interest increases by the same factor. Consequently, frequencies above $0.6 \approx 0.8$ kHz and up to 40 kHz are important during a test with a 1:10 scale model.

The effectiveness of the acoustic lining is defined by its geometry and construction materials. The lowest frequency

Fig. 7 Open-jet test section with anechoic plenum of DNW-NWB

at which the absorption is effective (cutoff frequency) is inversely proportional to the height of the wedges. For example, 0.8 m high wedges made from mineral wool covered by glass-reinforced fibre fabric have a typical cutoff frequency close to $100 \approx 200$ Hz and a reflection factor for plane waves at normal incidence smaller than 0.1 for frequencies above the cutoff frequency. At lower frequencies, the reflection factor increases rapidly. On the other hand, the cutoff frequency of a 0.2 m thick flat panel made from the same combination of materials is approximately 425 Hz.

When increasing the frequency of the sound, the most commonly encountered noise transmission problems are those resulting from sound reflections and sound leakages. Leaks through narrow gaps tend to be significant in the frequency range above approximately 2 kHz. Reflections on the other hand occur on every hard surface. The minimum area to create a sound reflection decreases while increasing the sound frequency. A generally accepted rule defines it to a quarter wavelength of the highest sound frequency of interest. This corresponds to an area of about 2 mm × 2 mm for a sound frequency around 40 kHz. Although unrealistic, this rule shows that every small structural surface inside the plenum that must be acoustically protected. If not properly acoustically treated, small gaps resulting from moving parts (like doors, moving walls, detachable ceilings, etc.), auxiliary elements (like ladders, walking platforms, lifting cranes, etc.) and interior lightning systems can produce undesired sound reflections and leakages that deviates the acoustic conditions inside the plenum from those registered in a pure acoustic free field.

However, there are cases in which it is impossible to hide all solid structures. These cases include all mechanical structures that are directly exposed to high flow velocities and structures that need to keep a defined aerodynamic shape, like model and inflow microphone supports and the wind tunnel collector. All these cases share a common point. The resulting interaction between the highly turbulent flow and the solid surfaces constitutes a major source of broadband noise.

Nishimura [20] investigated this phenomenon and demonstrated that vortex interaction-induced noise from a turbulent flow that impinges on a solid body can be significantly reduced when the latter is covered with pile fabrics. Pile fabrics are a type of cloth material with fine and high-density fibres and can be found in different thicknesses and structures. The purpose of using pile fabrics is to attenuate the near-wall flow vorticity. When vortices collide with pile fabrics, their kinetic energy is gradually reduced by the interaction with the fibres. As a result, the rapid deceleration of the flow near the wall does not occur and dipole-type noise is reduced. Another study compared different types of cloths and showed that the noise reduction highly depends on the structure of the pile fabric. A maximum sound pressure level

broadband noise reduction of up to 15 dB was observed compared with the same untreated hard surface [25]. This finding corresponds well with the results presented by Nishimura [20].

The acoustic characteristics of an anechoic plenum in wind-off conditions can be assessed utilizing the methods described in a series of international standards on room acoustics [42, 44, 45]. In most cases, these standards are the same ones chosen to certify the acoustic quality of the anechoic plenum. When applying these norms to the aerodynamic wind tunnel design, it is reasonable to compare the anechoic plenum to an anechoic chamber. This analogy suggests removing the collector from the plenum and covering both contraction and diffusor openings with acoustic lining for the in situ tests of the acoustic insulation and damping characteristics.

The requirements on the airborne acoustic insulation the of anechoic plenum walls are defined by weighted sound reduction indices [45]. Quantities such as noise absorption and sound transmission through wall partitions are fundamentally related to sound power. Therefore, sound intensity, or sound power, is a reliable quantity to be evaluated and provides an alternative approach for assessing the airborne sound insulation through walls. Measurement of the sound transmission through wall partitions between two rooms can be carried out in the laboratory or in situ. In the source room, a sufficiently diffuse sound field must be assumed. An easy way to achieve this is to distribute one or more noise sources away from the wall, so the portion of direct sound from the sound source to the wall is not significant in relationship to the portion of the diffuse sound.

The sound power passing through a surface can be related to the spatial averaged sound pressure level measured at the surface. Thus, the sound power incident on the wall is calculated based on sound pressure level measurements in the source room. The spatial averaging can be realized by either sweep measurements or by discrete point measurements over the entire wall that separates both source and receiving room. In the receiving room, the sound power transmitted through a wall partition is obtained using a similar type of measurement over the wall partition area. Finally, the apparent sound reduction index is defined as:

$$
R'_I = \left[\left(L_p\right)_{\text{inc}} - 6 + 10\log\left(\frac{A}{A_0}\right) \right] \\
- \left[\left(L_p\right)_{\text{trs}} + 10\log\left(\frac{A_p}{A_0}\right) \right],
\tag{8}
$$

where $\left(L_p\right)_{\text{inc}}$ and $\left(L_p\right)_{\text{trs}}$ is the sound pressure level measured in the source and receiving room, respectively.

In the case of an aeroacoustic wind tunnel, the rooms adjacent to the anechoic chamber are used as source rooms,

whereas the anechoic chamber is the receiving room. In conclusion, the anechoic plenum must be designed in such a way as to maximize the apparent sound reduction index of all the side walls, floor and ceiling of the plenum. This way, the acoustic isolation of the test section against external noise is maximized.

The damping effectiveness of an anechoic plenum provides a direct comparison between the acoustic conditions inside the plenum and those of a perfect acoustic free field. Therefore, it is evaluated comparing acoustic measurements at N positions along predefined acoustic propagation paths inside the plenum against the theoretically predicted sound pressure level for a sound propagation in the free-field. The sound pressure level at the measurement distance r_i for the ideal free-field propagation is modelled by the optimal reference method [44] according to the following equation:

$$L_p(r_i) = 20 \log \left(\frac{a}{r_i - r_0} \right),$$ (9)

where

$$a = \frac{\left(\sum_{i=1}^{N} r_i \right)^2 - N \sum_{i=1}^{N} r_i^2}{\sum_{i=1}^{N} r_i \sum_{i=1}^{N} 10^{-0.05 L_{p_i}} - N \sum_{i=1}^{N} \left(r_i 10^{-0.05 L_{p_i}} \right)}$$ (10)

and

$$r_0 = -\frac{\sum_{i=1}^{N} r_i \sum_{i=1}^{N} \left(r_i 10^{-0.05 L_{p_i}} \right) - \sum_{i=1}^{N} r_i^2 \sum_{i=1}^{N} 10^{-0.05 L_{p_i}}}{\sum_{i=1}^{N} r_i \sum_{i=1}^{N} 10^{-0.05 L_{p_i}} - N \sum_{i=1}^{N} \left(r_i 10^{-0.05 L_{p_i}} \right)}.$$ (11)

Here, it is considered that the acoustic and the geometric centre of the sound source may not coincide. The collinear offset between the two is estimated based on the measured sound pressure level along the propagation path using the regression (11). This value describes the deviation of the acoustic centre of the sound source from the geometrically defined one. Reference [44] does not define a limit for the collinear offset, however, if this value exceeds a certain threshold it can be assumed with certainty that the free-field conditions are not fulfilled inside the anechoic plenum. As a first approximation, one can consider the collinear offset to be limited to 0.2 m or to double wavelength of the tested frequency, whichever is achieved first. A multi-frequency tonal acoustic source is used as test signal, with frequencies corresponding to approximately the centre frequency of the one-third octave bands within the frequency range of interest. On one hand, the sound source is required to ensure a minimum signal-to-noise ratio of 10 dB at all microphone positions. On the other hand, the sound source must radiate a spherical sound wave as specified in Ref. [44]. Additionally, the sound power level of the sound source must not change during the measurement time of one propagation path. The

control of the sound power stability of the sound source is made by means of a stationary microphone during the measurements.

The acoustic measurements must also account for the atmospheric absorption inside the plenum and consequent sound pressure level attenuation along the propagation paths. For simple tones, the attenuation due to the atmospheric absorption $\left(\Delta L_p \right)_{atm}$ is given in terms of an attenuation coefficient as a function of four variables: the frequency of the sound, temperature, humidity and pressure of the air [40]. Consequently, the acoustic measurements along the propagation paths must be followed by measurements of the ambient pressure, air temperature and relative air humidity. The acoustic damping effectiveness of the anechoic plenum is finally defined at each measurement location as follows:

$$\Delta L_{p_i} = L_{p_i} + \left(\Delta L_{p_i} \right)_{atm} - L_p(r_i).$$ (12)

The lower the value, the closer the acoustic propagation of the sound inside the anechoic chamber is to the ideal free-field condition. It should be stressed that the deviation from the ideal free-field condition is evaluated as a function of the sound frequency, the position of the sound source and the measurement paths. Regarding the two last parameters, room acoustics require that the sound source is located in the centre of the room. Starting from the sound source, four measuring paths should run diagonally into the corners of the room. Additionally, one measuring path can be chosen arbitrarily. In a wind tunnel, it is useful to make some modifications to the standard procedure. The sound source must be located at the usual position of the test model regardless of the geometry of the anechoic chamber. The propagation paths must be defined while considering the most common microphone positions (free-field microphones, phased microphone arrays, etc.) during the wind tunnel measurements.

The results of the acoustic damping test only indicate deviations from the ideal free field. It is not possible to extract information about the reasons for those deviations. For example, they can be related to insufficient sound absorption of the acoustic lining or sound reflections on both hard and semi-hard surfaces. To identify possible sources of reflection, new acoustic methods such as the room impulse response method can be implemented. In the room impulse response method, the sound source at the origin of the propagation paths is substituted by a time-pulsed, high-pass filtered pink noise acoustic source [43]. The impulse response is evaluated in the time domain for every microphone position in the propagation path. To improve the clarity of the results, the impulse response along one path is commonly presented in a scalar map plot referred to as a reflectogram. Figure 8 shows an example of a reflectogram measured inside an anechoic plenum along an arbitrary acoustic propagation path. In the figure, the first oblique,
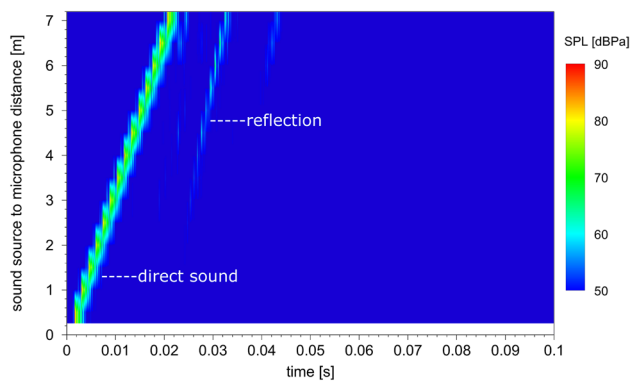
Fig. 8 Example of a spectrogram obtained by the impulse response method along an acoustic propagation path inside an anechoic plenum

Fig. 9 Overall background noise pressure level in different aeroacoustic wind tunnels in comparison with the same measured in a typical aerodynamic wind tunnel [29]

brighter line corresponds to the direct sound. This line is found in all reflectograms and is associated with the direct propagation of the sound wave along the path. Therefore, its slope is directly proportional to the propagation velocity, i.e., to the speed of sound. The second oblique line indicates a weak reflection from a flat surface. In a reflectogram, all impulse responses are normalised by the amplitude of their individual direct sound to remove the distance-related attenuation of the sound pressure level.

8 Performance measurements

The overall background sound pressure level and the pulsating coefficient are the most recognised quantities to determine the acoustic performance of an aeroacoustic wind tunnel in wind-on conditions. They are of special relevance because they provide the background noise level in the test section within the entire flow velocity range of the wind tunnel. Consequently, they define the signal-to-noise ratio for the measurements described below.

Figure 9 shows the overall background sound pressure level inside the anechoic plenum of a group of aeroacoustic wind tunnels as a function of the flow velocity. The plot shows that the background noise level inside the test section of an acoustically oriented wind tunnel design is typically 30 dB(A) lower, or more, than that measured in a classic aerodynamic wind tunnel. This value continues to decrease while the design tools are developed, especially the numerical ones. The most modern aeroacoustic wind tunnels designed with the highest level of development tools in the field of aerodynamic and acoustic show a background noise reduction of almost 50 dB(A). It should be emphasised, that the comparison between the overall background noise of different wind tunnels should be performed only if both the size of the wind tunnels and the position, or distance, of the microphone relative to the test section are comparable. All
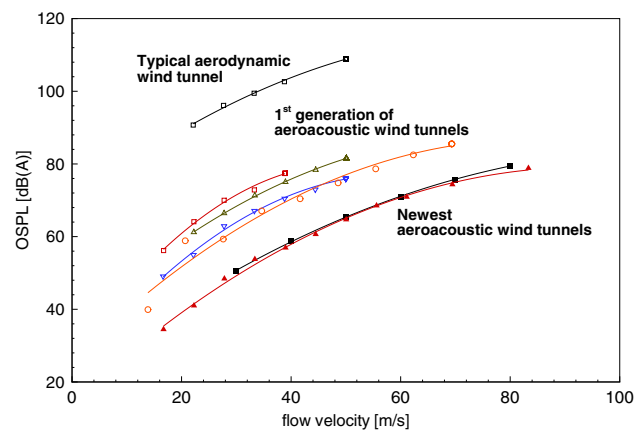
results shown in Fig. 9 were measured using a similar methodology as described in subsequent paragraphs. The distance of the microphone to the tunnel axis was approximately 6 m.

The overall background sound pressure level inside the anechoic plenum is measured as a function of the flow velocity in the absence of any test model and should consider the contribution of all acoustic frequencies from approximately 20 Hz up to 20 kHz. The measurements are standardly performed using a free-field microphone outside of the flow at a predefined distance from the wind tunnel axis. The microphone should be positioned perpendicular to the flow and aligned with the most common position of the test model. In most cases, the intersection between the wind tunnel model rotating table axis and the flow axis is used to represent this position. The selection of the microphone, the signal acquisition and post-processing systems must guarantee an accurate reconstruction of the measured acoustic signal in the form of a one-third octave band spectrum from the one-third octave band centred at 20 Hz up to 20 kHz. It is common practice to apply an *A*-weighted filter to the output signal of the microphone to give more weight to the sound frequencies of interest for human hearing and to attenuate the influence of both very low and very high acoustic frequencies [41]. With the inclusion of this filter, the evaluation of the background noise becomes very robust and provides very comparable results even when the measured frequency range has slightly different boundaries. As a consequence of the small scale of the test models, the *A*-weighted filter must only be skipped for very small aeroacoustic wind tunnels because of the shift of the frequencies of interest towards the high frequencies.

Finally, the overall background sound pressure level is calculated integrating the sound pressure level over the entire frequency spectrum. If the one-third octave band spectrum is used for that purpose, it corresponds to the

summation of the noise level, in decibels, of all frequency bands between the 13th and the 43th [41], inclusive, according to the following equation:

$$L_{\text{p,OSPL}} = 10 \log \sum_{i=13}^{43} 10^{\frac{L_{\text{p}i}}{10}}.$$ (13)

The pulsating coefficient provides a comparison between the magnitude of the low-frequency pressure fluctuations inside the anechoic plenum and the dynamic pressure in the free flow. When its magnitude exceeds a certain threshold, pressure fluctuations of low frequency lead to pulsating problems inside the wind tunnel with negative mechanical and acoustic consequences (see also Sect. 5). The frequency range of interest for the wind tunnel pulsation is located in the lower part of the frequency spectrum, typically between 1 Hz and 20 Hz.

The evaluation of the pulsating coefficient starts with the measurement of the overall sound pressure level, in dB(Z), within the lower frequency range. This should be performed with a microphone outside the flow at the same position as for the background noise measurements inside the anechoic chamber. Special attention must be paid to the selection of the microphone and filters to be used in the conditioning of the signal, because all the frequencies of interest during this measurement are smaller than 20 Hz. The overall sound pressure level can be calculated based on the narrow band spectrum of the measured acoustic signal after the logarithmic summation of all narrow bands within the frequency range from 1 up to 20 Hz. In this process, one must correct the results for the spectral leakage introduced by the windowing during the fast Fourier transformation. For a Hanning window, the noise equivalent bandwidth is equal to $1.5\Delta f$ which corresponds to the worst case amplitude error equal to 1.76 dB.

Finally, the pulsating coefficient is defined as:

$$C_{\text{p,RMS}} = \frac{p_0 10^{\frac{L_{\text{P,OSPL}}}{20}}}{\frac{1}{2}\rho U^2},$$ (14)

where p_0 is the reference pressure used in the computation of the sound pressure level (equal to 20 μPa) and ρ is the density of the air. The latter is calculated based on the meteorological information at the moment of the measurements.

Pulsating coefficient measurements are rarely reported for classic aerodynamic wind tunnels. This is because very low-frequency pressure fluctuations and their minimization are not considered a priority during their design. At best, the pumping effects are mitigated after the wind tunnel design using a posteriori solution if the low-frequency fluctuations in the test section are registered to be too big. For this reason, it is not uncommon to register pulsating
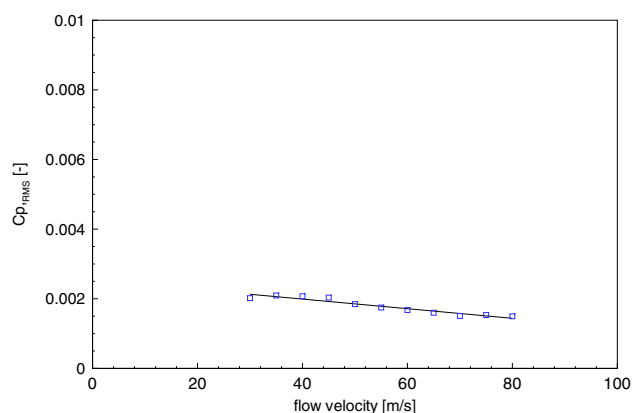
Fig. 10 Pulsating coefficient result in a modern aeroacoustic wind tunnel (DNW-NWB)

coefficients of about 0.02 or more in classic aerodynamic wind tunnels.

Conversely, aeroacoustic wind tunnels must be designed to minimize the pulsating coefficient and consequently any pumping effect in the test section and airline. Recent experience shows that low-frequency pressure fluctuations in a well-designed aeroacoustic wind tunnel are very small, typically lower than 1 % of the dynamic pressure inside the free flow. In terms of the pulsating coefficient, this represents a value smaller than 0.01. For this reason, this value is commonly accepted as the standard requirement for current and future aeroacoustic wind tunnel designs. Notwithstanding this requirement, the aeroacoustic wind tunnel design is so advanced nowadays that some of the most modern aeroacoustic wind tunnels have pulsating coefficients smaller than 0.002, as shown in Fig. 10.

References

1. Becker, K., Heitkamp, K., Kgeler, E.: Recent progress in a hybrid-grid CFD solver for turbomachinery flows. In: Proceedings of the 5th European Conference on Computational Fluid Dynamics ECCOMAS CFD 2010, Lisbon (2010)
2. Bertram, M., Deines, E., Mohring, J., Jegorovs, J., Hagen, H.: Phonon tracing for auralization and visualization of sound. In: Proceedings of IEEE Visualization (2005)
3. Broszat, D., Selic, T., Marn, A.: Verification of the inverse cut-off effect in a turbomachinery stage—Part 1—numerical results. In: 18th AIAA/CEAS Aeroacoustics Conference, Colorado Springs, Colorado (2012)
4. Broszat, D.U., Selic, T., Marn, A.: Verification of the inverse cut-off effect in a turbomachinery stage—Part 2—comparison to experimental results. In: 19th AIAA/CEAS Aeroacoustics Conference, Berlin (2013)
5. Brown, K., Devenport, W., Borgoltz, A.: Exploiting the characteristics of Kevlar-Wall wind tunnels for conventional aerodynamic measurements. In: AIAA AVIATION 2014—30th AIAA Aerodynamic Measurement Technology and Ground Testing Conference, Atlanta, Georgia (2014)

6. Camargo, H., Remillieux, M., Burdisso, R., Crede, E., Devenport, W.: The Virginia Tech stability wind tunnel from an aerodynamic into an aeroacoustic facility. In: 19th International congress on acoustics, Madrid (2007)

7. Cremer, L., Mueller, H.A.: Principles and Applications of Room Acoustics, vol. 1. Peninsula Publishing, Newport Beach (2016) **(ISBN 0932146732)**

8. Eisinger, F.L., Sullivan, R.E.: Unusual acoustic vibration in heat exchanger and steam generator tube banks possibly caused by fluid-acoustic instability. J Eng Gas Turbines Power **115**(2), 411–417 (1993)

9. Envia, E., Nallasamy, M.: Design selection and analysis of swept and leaned stator concept. J. Sound Vib. **228**(4), 793–836 (1999)

10. Gurin, S., Moreau, A., Tapken, U.: Relation between source models and acoustics duct modes. In: 16th AIAA/CEAS Aeroacoustics Conference, Miami, Florida (2009)

11. Gurin, S., Moreau, A.: Accounting for sweep and lean in the design-to-noise of rotor-stator stages. In: Proceedings of the DAGA Conference, Berlin (2010)

12. Holthusen, H., Bergmann, A.: Investigations and measures to improve the acoustic characteristics of the German-Dutch Wind Tunnel DNW-LLF. In: 18th AIAA/CEAS Aeroacoustics Conference, Colorado Springs, Colorado (2012)

13. Jensen, H.W.: Realistic Image Synthesis Using Photon Mapping. A.K. Peters Ltd, Natick (2001) **(ISBN 1568811470)**

14. Jensen, H.W., Christensen, N.J.: Photon maps in bidirectional Monte Carlo ray tracing of complex objects. Comput Graph **19**(2), 215–224 (1995)

15. Martin, R.M., Brooks, T.F., Hoad, D.R.: Reduction of background noise induced by wind tunnel jet exit vanes. AIAA J **23**(10), 1631–1632 (1985)

16. Melber-Wilkending, S., Bergmann, A.: Aeroacoustic optimization of the NWB airline and turning vanes based on high fidelity CFD and acoustic simulation. In: 18th AIAA/CEAS Aeroacoustics Conference, Colorado Springs, Colorado (2012)

17. Moreau, A., Enghardt, L.: A first step towards a parametric model for fan broadband and tonal noise. In: Proceedings of the DAGA Conference, Dresden, Germany (2008)

18. Moreau, A., Gurin, S.: Development and application of a new procedure for fan noise prediction. In: 16th AIAA/CEAS Aeroacoustics Conference, Stockholm (2010)

19. Moreau, A., Gurin, S.: Similarities of the free-field and in-duct formulations in rotor noise problems. 17th AIAA/CEAS Aeroacoustics Conference, Portland, Oregon (2011)

20. Nishimura, M., Kudo, T., Nishioka, T.: Aerodynamic noise reducing techniques by using pile-fabrics. In: 5th AIAA/CEAS Aeroacoustics Conference, Bellevue, WA (1999)

21. Paidoussis, M.P.: Flow-induced vibrations in nuclear reactors and heat-exchangers. In: Naudasher, E., Rockwell, D. (eds.) Practical Experiences with Flow-Induced Vibrations. Springer, New York (1980)

22. Papenfuss, H.D. et al.: Lowering the turbulence level in an open-jet wind tunnel by novel adjustable jet-exit vanes. In: FVP Symposium on Aerodynamics of Wind Tunnel Circuits and their Components, CP-585, Moscow (1996)

23. Parker, R.: Resonance effects in wake shedding from parallel plates: some experimental observations. J. Sound Vib. **5**(2), 330–343 (1966)

24. Parker, R.: Resonance effects in wake shedding from parallel plates: calculation of resonant frequencies. J. Sound Vib. **5**(2) (1967)

25. Pott-Pollenske, M., von Heesen, W., Bergmann, A.: Acoustic pre-examination work and characterization of the low-noise wind tunnel DNW-NWB. In: 18th AIAA/CEAS Aeroacoustics Conference, Colorado Springs, Colorado (2012)

26. Remillieux, M.C., Crede, E.D., Camargo, H.E., Burdisso, R.A., Devenport, W.J., Rasnick, M., Van Seeters, P., Chou, A.: Calibration and demonstration of the new Virginia Tech anechoic wind tunnel. In: 14th AIAA/CEAS Aeroacoustics Conference, Vancouver, British Columbia Canada (2008)

27. Roeber, N., Andres, S., Masuch, M.: HRTF simulations through acoustic Raytracing, Tech. Rep., Fakultaet fuer Informatik, Otto-von-Guericke Universitaet Magdeburg (2006)

28. Roeber, N., Kaminski, U., Masuch, M.: Ray acoustics using computer graphics technology. In: Proceedings of the 10th International Conference on Digital Audio Effects, Bordeaux (2007)

29. Schneider, S., Wiedemann, J., Wickern, G.: Das Audi-Windkanalzentrum, Aerodynamik des Kraftfahrzeugs, Haus der Technik, Essen, Germany (1998)

30. Seiferth, R.: Vorausberechnung und Beseitigung der Schwingungen von Freistrahl-Windkanlen, Aerodynamische Versuchsanstalt, Goettingen, Germany (1946)

31. Sijtsma, P.: CLEAN based on spatial source coherence. Int. J. Aeroacoust. **16**(4), 357–374 (2007)

32. Sijtsma, P., Merino-Martinez, R., Malgoezar, A., Snellen, M.: High-resolution CLEAN-SC: theory and experimental validation. Int. J. Aeroacoust. **16**(4–5), 274–298 (2017)

33. Voss, C., Becker, K., Lawerenz, M.: Multi-objective optimization in axial compressor design using a linked CFD-Solver, In: ASME Turbo Expo 2008 Conference (2008)

34. von Heesen, W.: Abnormal high-level tonal noise in axial-flow fans. In: 4th AIAA/CEAS Aeroacoustics Conference, Toulouse (1998)

35. Waudby-Smith, P., Ramakrishnan, R.: Wind tunnel resonances and Helmholtz resonators. Can. Acoust. **35**(1), 3–11 (2007)

36. Welsh, M.C., Stokes, A.N., Parker, R.: Flow-resonant sound interaction in a duct containing a plate—Part I: semi-circular leading edge. J. Sound Vib. **95**(3), 305–323 (1984)

37. Wickern, G., von Heesen, W., Wallmann, S.: Wind tunnel pulsations and their active suppression. SAE Technical Paper 2000-01-0869 (2000)

38. Woodward, R., Hughes, C., Berton, J.: Benefits of swept and leaned stators for fan noise reduction. In: 37th Aerospace Sciences Meeting, Reno, Nevada (1999)

39. Woodward, R., Hughes, C., Jeracki, R., Miller, C.: Fan noise source diagnostic test: Far-field acoustic results. In: 8th AIAA/CEAS Aeroacoustics Conference, Breckenridge, Colorado (2002) International standards:

International standards

40. ISO 9613-1:1993: Attenuation of sound during propagation outdoors—Part 1: calculation of the absorption of sound by the atmosphere. International Organization for Standardization (1993)

41. ISO 266:2003: Normal equal-loudness-level contours. International Organization for Standardization (2003)

42. ISO 15186-2:2003: Measurement of sound insulation in buildings and of building elements using sound intensity—Part 2: field measurements. International Organization for Standardization (2003)

43. ISO 18233:2006: Application of new measurement methods in building and room acoustics. International Organization for Standardization (2006)

44. ISO 3745:2012: Determination of sound power levels and sound energy levels of noise sources using sound pressure—precision methods for anechoic rooms and hemi-anechoic rooms. International Organization for Standardization (2012)

45. ISO 717-1:2013: Rating of sound insulation in buildings and of building elements—Part 1: airborne sound insulation. International Organization for Standardization (2013)